Dependence of climate states of gray atmosphere on solar constant: From the runaway greenhouse to the snowball states

Masaki Ishiwatari

Faculty of Environmental Earth Science, Hokkaido University, Sapporo, Japan

Kensuke Nakajima

Faculty of Sciences, Kyushu University, Fukuoka, Japan

Shin-ichi Takehiro

Research Institute for Mathematical Sciences, Kyoto University, Kyoto, Japan

Yoshi-Yuki Hayashi

Graduate School of Sciences, Kobe University, Kobe, Japan

submitted to *JGR* 04 April, 2006, revision 28 September, 2006, 2nd revision 15 January, 2007, 3rd revision 03 April, 2007, accepted by *JGR* 02 May, 2007, published 13 July, 2007

Citation: Ishiwatari, M., K. Nakajima, S. Takehiro, and Y.-Y. Hayashi (2007), Dependence of climate states of gray atmosphere on solar constant: From the runaway greenhouse to the snowball states, J. Geophys. Res., 112, D13120, doi:10.1029/2006JD007368.

Abstract

Multiple equilibrium solutions of a gray atmosphere are investigated for various values of the solar constant. Two types of models are utilized in order to conduct a comparative study: a general circulation model with simplified physical processes (GCM) and a one-dimensional energy balance model (EBM). For intermediate values of solar constant, both of the models indicate the existence of multiple solutions that include the runaway greenhouse state in addition to the globally ice-covered state and the partially ice-covered state. In the GCM results, there is no partially ice-covered state with the ice line latitude lower than 22°. This indicates that the large ice cap instability discussed in previous EBM studies also occurs in GCM. Compared to the results of EBM, the ice line of the partially ice-covered state of GCM reaches lower latitudes. The appearance of the large ice cap instability in our GCM is impeded by condensation heating at the ice lines. The efficient latitudinal heat transport in the Hadley cell is considered to be a contributing factor to this delay in ice cap expansion.

1 Introduction

The solar constant is one of the most important parameters that determine the climate of terrestrial planets. A state of mild climate like that of the present Earth vanishes when the value of solar constant changes by several tens of percent, as reviewed briefly below.

When the value of solar constant is decreased from that of the present earth, the globally ice-covered state emerges. One-dimensional energy balance models (EBMs) show that a slight decrease in solar constant results in ice-covered Earth [*Budyko*, 1969; *Sellers*, 1969]. With the solar constant set at the value of present Earth, Budyko's EBM gives multiple equilibrium solutions: a globally ice-covered equilibrium solution and two types of partially ice-covered solutions [1]. The partially ice-covered solution whose ice line is located at higher latitudes is stable and is regarded as the climate regime of the present Earth. In contrast, the partially ice-covered solution whose ice line is located at lower latitudes is unstable [*Held and Suarez*, 1974; *Cahalan and North*, 1979]. This instability is referred to as the large ice cap instability.

Ice-covered solutions are also obtained in experiments using general circulation models (GCMs). Inspired by the snowball Earth hypothesis proposed by *Hoffman et al.* [1998], *Baum and Crowley* [2001] performs numerical experiments with a coupled atmosphere-ocean GCM and exemplifies the possibility of the appearance of the globally ice-covered state under the climate conditions of the Neoproterozoic age. In order to gain insights on the climate on ancient Mars, *Abe et al.* [2005] explores possible climate states for a wide range of parameters with a terrestrial GCM, and shows that the globally ice-covered state emerges with decreased solar

[1]Note that the number of equilibrium solutions and their stability depend on the setup of EBM. The EBM of *Sellers* [1969] has an unstable equilibrium solution with a small ice cap. The instability is referred to as the small ice cap instability [*North*, 1984].

constant regardless of the obliquity of the planet.

When the value of the solar constant is increased, the runaway greenhouse state emerges and the atmosphere cannot reach an equilibrium state until the entire ocean evaporates. One-dimensional radiative-convective equilibrium models show that there exists an upper limit to the value of outgoing longwave radiation (OLR) emitted from the top of the atmosphere on a planet with ocean [*Komabayashi*, 1967; *Ingersoll*, 1969; *Nakajima et al.*, 1992]. When the incident energy flux exceeds this upper limit, no equilibrium state exists. Indeed, experiments with GCMs employing a value of solar constant larger than this limit demonstrate that the runaway greenhouse state is characterized by continuous increase both in the atmospheric temperature and water vapor amount [*Ishiwatari et al.*, 1998, 2002].

It is also known that some one-dimensional radiative-convective models have multiple equilibrium solutions. As in EBM, the inclusion of ice-albedo feedback produces multiple equilibrium solutions [*Li et al.*, 1997]. Multiple equilibrium solutions also result from the inclusion of the hydrologic cycle [*Rennó*, 1997; *Sugiyama et al.*, 2005]. For certain values of incoming solar radiation flux, *Rennó* [1997] shows that two types of stable equilibrium solutions can be obtained: one being an optically thin equilibrium state and the other being an optically thick equilibrium state. *Sugiyama et al.* [2005] show that the two types of solutions obtained by *Rennó* [1997] exist if the derivative of relative humidity with respect to surface temperature is larger than a certain critical value. It should be emphasized that the introduction of a hydrologic cycle, in general, may change the dynamical branch structure of the solutions, although no statistically equilibrium state which can be regarded as corresponding to the optically thick equilibrium solutions discussed by *Rennó* [1997] and *Sugiyama et al.* [2005] is observed in the results of GCM experiments performed by *Ishiwatari et al.* [2002].

In previous studies, investigations on the climatic dependence on the value of solar constant are carried out employing models that can only represent either the runaway greenhouse state or the ice-covered state. In the EBMs of *Budyko* [1969] and *Sellers* [1969], OLR is given as a linear function of surface temperature. Hence, there is no upper limit to OLR, and so the runaway greenhouse state cannot be described. There is a possibility that the stability of solutions for a model which allows the occurrence of the runaway greenhouse state differs from those of previous EBMs, since the dynamical branch structure of the solutions may change.

In this article, the branch structure of climatic solutions ranging from the ice-covered state to the runaway greenhouse state is examined using an EBM and a GCM of a gray atmosphere having the same radiation properties. By adopting the gray atmosphere, our EBM enables us to draw a branch diagram of climate regime which includes the runaway greenhouse state. The use of the GCM allows us to explore climate solutions with explicit representation of the atmospheric circulation and water vapor transport. The incorporation of atmospheric motion may result in a different climate regime diagram from that obtained by EBM. By comparing the solutions of EBM and GCM over a wide range of solar constants, we can determine whether a branch obtained by EBM has a corresponding one in the climate regime diagram obtained by GCM, and vice versa. The aim of this study is to produce a "GCM version of the Budyko-Sellers diagram."

2 Model

The GCM utilized here is AGCM5.3 of GFD DENNOU CLUB. It is the same model which is used by *Ishiwatari et al.* [1998, 2002]. Except for the incorporation of three-dimensional atmospheric motion, the system is basically equivalent to the

one-dimensional radiative-convective equilibrium model of *Nakajima et al.* [1992] in which the existence of radiation limits is clarified and the runaway greenhouse state is described in terms of them. It is the most basic model for a GCM; we have chosen to retain the simplicity of the model for making an straightforward extension of previous studies to three-dimensional models. The basic features of our GCM are briefly summarized as follows. The atmosphere consists of a condensable component (water vapor) and a noncondensable component (dry air). Only water vapor absorbs and emits longwave radiation. The absorption coefficient of water vapor is constant and independent of wavelength. Dry air is assumed to be transparent. Cumulus convection is parameterized by a convective adjustment scheme [*Manabe et al.*, 1965]. Condensed water is removed from the system immediately without cloud formation. The radiative effects of clouds and the scattering of radiation are excluded. Vertical diffusion is represented by the Yamada-Meller Level-II scheme. The entire surface is assumed to be a "swamp ocean"; heat capacity is zero and wetness is unity [*Delworth and Manabe*, 1988]. Heat transport by the ocean is excluded. The surface albedo of regions whose surface temperature is below the freezing point, 263K as adopted by *Budyko* [1969], is 0.5. Otherwise, the surface albedo is zero. Neither snow accumulation, ice mass budget, nor sea ice migration are considered. Latent heat of fusion is also excluded from the calculation. This simple model configuration permits the direct comparison of our GCM results with that of EBMs. The dynamical part of the GCM is represented by the pseudo spectral method in the horizontal direction, and by the finite difference method with σ coordinate in the vertical direction. The spectral truncation adopted here is the triangular truncation at wavenumber 21 (T21). The number of vertical levels is 16 for the cases where the value of solar constant, S, is smaller than 1450 Wm^{-2} and 32 for the cases where S is greater than 1450 Wm^{-2}. The

number of vertical levels is increased for the larger solar constant values, because the tropopause extends to higher altitudes. With this configuration of the model vertical levels, OLR is calculated to an accuracy of 5 Wm^{-2} [*Ishiwatari et al.*, 2002].

The EBM utilized here is the same as that of *North* [1975], except for the radiation scheme. The radiation scheme is the same as that used in our GCM described above, that is, the gray atmosphere of *Nakajima et al.* [1992]. By adopting this radiation scheme, the value of OLR is determined to be a function of the surface temperature on the basis of a one-dimensional radiative-convective equilibrium solution. The relative humidity is given as a fixed value of 60 %, which is obtained as a typical value in our GCM results [*Ishiwatari et al.*, 2002]. The meridional heat transport is calculated by the diffusion scheme of *North* [1975]. The value of the heat transport coefficient is 0.5 $\mathrm{Wm}^{-2}\mathrm{K}^{-1}$. The value is determined such that the EBM most closely reproduces the meridional temperature difference of the GCM in the ice-free case with $S = 1380$ Wm^{-2}. In addition to searching for the steady solutions for the EBM, time developments of the solutions are also calculated to investigate the existence of the runaway greenhouse state. In time-dependent problems, the value of heat capacity for a unit area is set to be 1 $\mathrm{JK}^{-1}\mathrm{m}^{-2}$. The value of heat capacity can be chosen arbitrary, since it does not affect the results of examination on the existence of the runaway greenhouse state, except for zero. Zero heat capacity cannot be adopted in the time-dependent EBM, since the tendency term of surface temperature vanishes and surface temperature becomes indefinite.

The value of solar constant S is varied in the range between 1200 Wm^{-2} and 2000 Wm^{-2}. The meridional distribution of incoming solar flux is given as the annual and daily averages of that evaluated using the present terrestrial orbital parameters. As for the GCM runs, four kinds of initial conditions are selected:

the isothermal (280K) state with constant specific humidity of 10^{-3}, a calculated runaway greenhouse solution at 1000 day obtained with S=1600 Wm^{-2}, a calculated partially ice-covered solution obtained with S=1300 Wm^{-2}, and a calculated globally ice-covered solution obtained with S=1000 Wm^{-2}. These values are arbitrary chosen. The equilibrium solutions of the EBM are obtained by the use of the Powell hybrid method in Minpack which is available at http://www.netlib.org. The runaway solutions of the EBM are obtained by solving the time-dependent problem using an isothermal state having temperature of 330K or 600K as the initial conditions. These temperature values are also arbitrary chosen.

3 Results of EBM Experiments

Figure 1 shows the relationship between solar constant and ice line latitude of solutions obtained by the EBM. Ice line latitude at 90° corresponds to an ice-free solution, and 0° to a globally ice-covered solution. Crosses at 90° indicate nonequilibrium solutions where the system is in the runaway greenhouse state.

The gross feature of ice-covered solutions shown in Figure 1 is similar to the results of *Budyko* [1969] or *Sellers* [1969]. In our EBM, globally ice-covered solutions, indicated as branch α, are found for $S \leq 1903\mathrm{Wm}^{-2}$ (point A). One or multiple partially ice-covered solutions are found for $1306\mathrm{Wm}^{-2} \leq S \leq 1903\mathrm{Wm}^{-2}$, indicated by branches β, γ, and δ and critical points A, B, C, and D in Figure 1. Branch β intercepts globally ice-covered solutions (branch α) at point A ($S = 1903\mathrm{Wm}^{-2}$), and branch δ is connected with ice-free equilibrium solutions (branch ε) at point D ($S = 1436\mathrm{Wm}^{-2}$). In contrast to the results of *Budyko* [1969] or *Sellers* [1969], the branch connections in partially ice-covered solutions and ice-free solutions in the present study display complicated features, the details of which will be explained below.

The branch structure of ice-free equilibrium solutions in Figure 1 displays different features from the results of *Budyko* [1969] or *Sellers* [1969]. Since the runaway greenhouse state is allowed to emerge in our model, an upper limit to S must exist in order for the ice-free equilibrium solutions to exist. Point E ($S = 1441.2\mathrm{Wm}^{-2}$) is the critical point for the ice-free equilibrium state; no ice-free equilibrium solution can be found in our EBM at any larger values of S. The detail of the branch structure of ice-free equilibrium solution which cannot be recognized in Figure 1 will be shown later, in Figure 2b. For the values of solar constant smaller than that of critical point E, there are two branches of ice-free equilibrium solutions; the first, branch ε is connected to the partially ice-covered solutions (branch δ) at point D, and the other, branch ζ is connected to the runaway greenhouse state at point F ($S = 1310\mathrm{Wm}^{-2}$). This is the lower limit of S for which the runaway greenhouse state can be found, and it is also the lower limit of S for which an ice-free equilibrium solution can exist. However, the ice-free equilibrium solutions on branch ζ are unstable, as will be explained later in this section.

The partially ice-covered solutions belong to two kinds of branches; one is branch γ in which the ice-covered area decreases with increasing S, and the other consists of two branches β and δ in which the ice-covered area increases with increasing S. As for the stability of the equilibrium solutions, the argument presented by *Cahalan and North* [1979] should also be applicable for our case since the difference between our radiative term and theirs is not expected to cause a significant difference in the radiative heating property of the partially ice-covered state. The solutions on branch γ are considered to be stable, while the solutions on branches β and δ are unstable. Change of stability occurs at the critical points indicated as point B ($S = 1306\mathrm{Wm}^{-2}$) and point C ($S = 1447.5\mathrm{Wm}^{-2}$). Branch δ has ice line latitudes higher than 69°, which is reached at point C, and branch β has ice line latitudes

lower than 28°, which is reached at point B. Following *North* [1984], the instability corresponding to branch δ whose ice line is located at higher latitudes is referred to as the small ice cap instability, and the instability corresponding to branch β whose ice line is located at lower latitudes is referred to as the large ice cap instability.

In order to clarify the branch configuration of the partially ice-covered state and the ice-free state, the relationship between solar constant S and global mean surface temperature $\overline{T_s}$ of the equilibrium solutions is plotted in Figure 2. Note that the runaway greenhouse state cannot be plotted in these panels, since global mean surface temperature is an increasing function of time for solutions in the runaway greenhouse state. The stable branch γ of the partially ice-covered state corresponds to the branch where global mean surface temperature increases with solar constant in Figure 2a that extends from point B ($\overline{T_s} = 258$K) to point C ($\overline{T_s} = 298$K). Branch β of the large ice cap instability corresponds to the branch extending from point B ($\overline{T_s} = 258$K) to point A ($\overline{T_s} = 254$K). On this branch, when the ice line latitude is far removed from the equator, global mean surface temperature decreases with the increase in solar constant within the range from point B to $S = 1450\mathrm{Wm}^{-2}$. When the ice line latitude becomes closer to the equator, global mean surface temperature increases slightly with an increase in solar constant within the range from $S = 1450\mathrm{Wm}^{-2}$ to point A. Nevertheless, the equilibrium solutions on this whole branch are locally unstable, as stated earlier.

The configuration of the branch of small ice cap instability is even more complicated. The transition area from the branch of small ice cap instability to the branch of ice-free solutions is enlarged in Figure 2b. Branch δ of small ice cap instability corresponds to the line segment that extends from point C to point D ($\overline{T_s} = 297$K). It connects to branch γ of the stable partially ice-covered solutions

at point C, and to branch ε of the ice-free solutions at point D. On branch δ, global mean surface temperature increases with increase in solar constant from point D, reaches a maximum of $\overline{T_s}$ =302K at S =1442Wm^{-2}, and then decreases with solar constant toward point C.

As mentioned earlier, the ice-free state in our EBM consists of two branches, branch ε and branch ζ shown in Figure 2b. Point E, $(S, \overline{T_s}) = (1441.2\text{Wm}^{-2}, 300.4\text{K})$, is a critical branch point. Branch ε is connected to branch δ of the unstable partially ice-covered state at point D, while branch ζ extends up to point F $(1310\text{Wm}^{-2}, 453\text{K})$, which is beyond the range of Figure 2b. As the value of solar constant increases, global mean temperature increases on branch ε, whereas it decreases on branch ζ. Almost all of the ice-free solutions plotted in Figure 2a belong to branch ζ; the ice-free solutions on branch ε are difficult to recognize in Figure 1 and Figure 2a, because of the superposition of other solutions.

The reason for the existence of two branches of the ice-free state in our EBM is best understood from the results of the one-dimensional radiative-convective equilibrium model. It is known that, in a one-dimensional equilibrium model that includes the same radiative process as that of our EBM, there exists two kinds of equilibrium solutions for a given value in a certain range of solar constant [*Nakajima et al.*, 1992]. One is the branch of solutions where an increase in solar constant is balanced by an increase in OLR, caused by an increase in surface temperature. The other is the branch of solutions where an increase in solar constant is balanced by an increase in OLR, caused by a decrease in atmospheric opacity due to the reduction in atmospheric water vapor content forced by a decrease in surface temperature. Branch ε of ice-free solutions in Figure 2b corresponds to the former branch of the one-dimensional radiative-convective equilibrium solutions, while branch ζ corresponds to the latter. $S = 1310$ Wm^{-2} at point F, which is the

lower limit of S for the emergence of the runaway greenhouse state, corresponds to the limiting value of OLR for cases with high surface temperature. On the basis of the stability argument on the one-dimensional radiative-convective equilibrium solutions, ice-free equilibrium solutions on branch ε are expected to be stable, while those on branch ζ are unstable. Our time-dependent calculations confirm that the ice-free equilibrium solutions on branch ζ are unstable. As is shown in Figure 1, for a given value of incoming solar flux, all equilibrium solutions on branch ζ coexist with a runaway greenhouse solution.

4 Results of GCM Experiments

Figure 3a shows the relationship between solar constant and ice line latitude of the statistically equilibrium solutions obtained by our GCM. The runaway greenhouse solutions found by the GCM are also plotted by crosses. The relationship between solar constant and global mean surface temperature of the statistically equilibrium solutions is shown in Figure 3b. In these figures, results for runs started from various initial conditions are all plotted. Partially ice-covered statistically equilibrium solutions are found for $1250\mathrm{Wm}^{-2} \leq S \leq 1570\mathrm{Wm}^{-2}$. Of these solutions, those for $1300\mathrm{Wm}^{-2} \leq S \leq 1570\mathrm{Wm}^{-2}$ are obtained from runs having the initial conditions of the isothermal atmosphere of 280K. Those for $1250\mathrm{Wm}^{-2} \leq S < 1300\mathrm{Wm}^{-2}$ are calculated starting from the partially ice-covered solution for $S = 1300\ \mathrm{Wm}^{-2}$, then by gradually decreasing the value of solar constant from $S = 1300\ \mathrm{Wm}^{-2}$. The latter solutions are labeled by P in Figure 3. Globally ice-covered statistically equilibrium solutions are obtained for $S \leq 1710\ \mathrm{Wm}^{-2}$. Note, however, that it is for $S \leq 1295\ \mathrm{Wm}^{-2}$ that the globally ice-covered state is obtained from runs having the initial condition of the isothermal atmosphere of 280K. The globally ice-covered solutions labeled by F in Figure 3 are obtained

from a globally ice-covered solution calculated with $S = 1000$ Wm^{-2}. From this initial condition, the globally ice-covered state is sustained up to $S = 1710$ Wm^{-2}. At $S = 1720$Wm^{-2}, all of the ice disappears and the runaway greenhouse state appears.

The partially ice-covered statistically equilibrium state of the GCM extends to smaller solar constant values and the corresponding ice line latitude reaches lower latitudes compared to those of the stable equilibrium solution for the EBM. As is shown in Figure 3a, the smallest value of solar constant for which a partially ice-covered statistically equilibrium solution is obtained by the GCM is $S = 1250$Wm^{-2}, with the ice line latitude of 22°. The corresponding value obtained by the EBM is $S = 1306$Wm^{-2}, with the ice line latitude at 28°. The ice line latitude of the GCM solution for $S = 1250$Wm^{-2} remains stable throughout the long integration period of over 60000 days, while no statistically equilibrium partially ice-covered solution can be found for $S = 1240$Wm^{-2}; only a globally ice-covered solution is obtained.

The reason why the GCM can maintain the partially ice-covered state at smaller values of solar constant compared to that of the EBM is the existence of the Hadley circulation. In the region of the Hadley circulation, very efficient heat exchange takes place in the meridional direction, and the temperature distribution in the troposphere tends to be latitudinally uniform. In contrast, the heat exchange between the Hadley circulation cells and regions at higher latitudes is comparatively inefficient, and so baroclinically unstable zones with latitudinal temperature gradient are formed [*Satoh*, 1994]. As the solar constant decreases, the ice line latitude eventually falls within the Hadley circulation. Then, the equatorward migration of ice line latitude slows down, since the solar flux supplied to the entire tropical region efficiently heats the area of the ice line latitudes due to the efficient thermal

mixing in the Hadley circulation. In our EBM, unlike that of *Lindzen and Farrell* [1977], the latitudinal heat transport is modeled simply as a function proportional to the temperature gradient; thus, the dependence of the efficiency of meridional heat transport on the dynamical difference of the circulation structure is not represented. When the ice line latitude reaches the lower latitudes, heat transport from the equatorial area decreases in the EBM because of the decrease in latitudinal temperature gradient.

The structure of the Hadley circulation of the partially ice-covered state with a large ice cap is different from the other cases. Figures 4 and 5 compare the temporal and zonal mean meridional structures of a statistically equilibrium state for the case with $S = 1380\mathrm{Wm}^{-2}$ where the ice line latitude is located at 40.8°, and for the case with $S = 1250\mathrm{Wm}^{-2}$ where the ice line latitude is located at 22°, respectively. The remarkable point is that the locations of the precipitation peaks for $S = 1250\mathrm{Wm}^{-2}$ are not at the equator but at the ice line latitudes (Figure 5a); little precipitation is observed at the equator. This sharply contrasts with the ordinary case exemplified for $S = 1380\ \mathrm{Wm}^{-2}$ (Figure 4a), where the precipitation peak is located near the equator. In line with the distribution of precipitation, the upward motion in the case of the $S = 1250\mathrm{Wm}^{-2}$ appears at the ice line latitudes, while downward motion appears at the equator (Figure 5b). Also note that the direction of the Hadley circulation for $S = 1250\mathrm{Wm}^{-2}$ is opposite to that for $S = 1380\mathrm{Wm}^{-2}$ (Figure 4b). As for energy transport, precipitation at the ice line latitudes for $S = 1250\mathrm{Wm}^{-2}$ is maintained by the latent heat transport from the equatorial latitudes, as shown by the solid line in Figure 5c. The transport of dry static energy, on the other hand, is equatorward as shown by the solid line in Figure 5d and contributes to the warming of the entire tropics. These also contrast with the ordinary case exemplified for $S = 1380\ \mathrm{Wm}^{-2}$ (Figures 4c and

4d), where the latent heat energy and dry static energy in the Hadley circulation are transported equatorward and poleward, respectively.

It seems that the large ice cap instability exists also in the climate system of our GCM. We could not find a statistically equilibrium partially ice-covered solution having an ice line latitude lower than 22°. The partially ice-covered solutions labeled by P in Figure 3a, whose ice line latitudes are located near 22°, can be obtained only when initial conditions are in the vicinities of the solutions. From an isothermal state with $T = 280$K, the system cannot reach the partially ice-covered solutions, and instead, ends up in the globally ice-covered state. There seems to be a critical point around $S = 1250\text{Wm}^{-2}$ and the ice line latitude of 22°, and the stability of the statistically equilibrium partially ice-covered state is weakened as this critical point is approached. On the other hand, the globally ice-covered solutions labeled by F in Figure 3a can be obtained only from a globally ice-covered solution. From an isothermal state of $T = 280$K, the system cannot reach the globally ice-covered solutions, and instead, ends up in either the partially ice-covered state or the runaway greenhouse state. There seems to be a critical point near $S = 1710\text{Wm}^{-2}$ of the globally ice-covered state, and the stability of the statistically equilibrium globally ice-covered state is weakened as this critical point is approached. These results suggest that an unstable branch is present in the GCM solutions.

As for the small ice cap instability, our GCM seems to lack any structure that clearly corresponds to that of the EBM. The time mean value of the ice line latitude for $S = 1560\text{Wm}^{-2}$ is 87°. The system reaches the ice-free state at $S = 1570$ Wm^{-2}. From these GCM results, it is hard to assert the existence of a nonvanishing, minimum size of the ice cap. The transition between the ice-free and the partially ice-covered statistically equilibrium states appears to be continuous.

As the value of solar constant increases and the ice line latitude recedes poleward, the fluctuation amplitude of the ice line latitude increases (Figure 6). These results seem to be consistent with the results of *Lee and North* [1995]. *Lee and North* [1995] obtains the continuous transition from partially ice-covered solutions to the ice-free solutions with GCM and noise-forced EBM.

The runaway greenhouse state of the GCM emerges for $S \geq 1600$ Wm^{-2} when the initial condition is the 280K isothermal state. When a runaway greenhouse solution is used as the initial condition, the range of S which maintains the runaway greenhouse state extends to the smaller S values. These correspond to the solutions marked with label R in Figure 3a, for which the runaway greenhouse solution obtained with $S = 1600$ Wm^{-2} is given as the initial condition. The runaway greenhouse state is maintained even when the value of solar constant is reduced to $S = 1300$ Wm^{-2}; global averaged surface temperature continues to increase. However, for the value of solar constant $S = 1280$ Wm^{-2}, surface temperature drops and the globally ice-covered state is reached. The smallest value of S which can maintain the runaway greenhouse state can be interpreted as the limiting value of OLR which is achieved in the case where the atmospheric water vapor amount is sufficiently increased in the one-dimensional radiative-convective model having a fixed value of tropospheric relative humidity [*Nakajima et al.*, 1992]. The limiting value of OLR is estimated as 330Wm^{-2} for tropospheric relative humidity of 60 %, which is the typical value obtained in the GCM. This estimation is in fairly good agreement with the lowest limit of the globally mean incoming solar flux that brings about the emergence of the runaway greenhouse state ($S/4$).

5 Summary and Discussions

The results obtained by our GCM suggest that the large ice cap instability also occurs in a three-dimensional system. We may speculate that there exists an unstable solution with an large ice cap whose ice line latitude is located between 22° and the equator. Such an unstable solution in the GCM, if it exists, will be difficult to find. The structure of the large ice cap instability of the GCM may be altered from that of EBM because of the existence of Hadley circulation in the GCM. The EBM of *Lindzen and Farrell* [1977], which takes into account the effect of Hadley circulation, may be useful in examining the contrast between the large ice cap instabilities of the GCM and the EBM in detail. However, we leave this theme for future studies. As for the small ice caps, our GCM yields statistically equilibrium states, which seems to indicate that, in our three-dimensional system, small ice cap instabilitiy does not exist. Our results are similar to those by *Lee and North* [1995]. Thus, we have confirmed that a clear counterpart of the small ice cap instability discussed in EBMs is not found in the GCM in which both the runaway greenhouse state and the ice-covered state are permitted. Since *Lee and North* [1995] predicts that the manifestation of small ice cap instability depends on the strength of noise forcing, a GCM experiment including the effect of the response time of ice cover might be an interesting subject. The thermal inertia of ice sheets may affect stability.

The statistically equilibrium states obtained by our GCM correspond to some of the equilibrium solutions appearing in the vertically one-dimensional radiative-convective models. The corresponding ones are the equilibrium solutions on the branch of increasing OLR with increase in surface temperature obtained by *Nakajima et al.* [1992], and the optically thin equilibrium solutions of *Rennó* [1997] and *Sugiyama et al.* [2005]. The GCM results of this study or of *Ishiwatari et al.*

[2002] do not seem to show any correspondences to the optically thick equilibrium solutions of *Rennó* [1997] and *Sugiyama et al.* [2005]. The difference lies in the dependence of relative humidity on surface temperature. In the optically thick equilibrium solutions of *Sugiyama et al.* [2005], relative humidity increases with increase in surface temperature, while, in the tropics of our GCM, relative humidity decreases [*Ishiwatari et al.*, 2002]. There is a possibility that the moistening efficiency of cumulus might affect the branch structure of solutions. *Rennó* [1997] mentions that the optically thick equilibrium solutions could not be found when convective adjustment scheme was utilized or when relative humidity was fixed in his one-dimensional radiative convective model. Solutions corresponding to the optically thick equilibrium solutions of *Rennó* [1997] and *Sugiyama et al.* [2005] might be obtained in the GCM if the cumulus parameterization scheme, which has a vigorous moistening effect against the drying in the Hadley circulation region, is utilized. However, it is unclear at this point whether the moistening effect of cumulus would be so efficient when surface temperature is increased.

Our GCM demonstrates that a runaway greenhouse state or a statistically equilibrium state can be realized for the same value of solar constant in the range of $1300 \leq S \leq 1570\mathrm{Wm}^{-2}$ depending on the choice of initial conditions. However, we have not been able to confirm the expectation of *Rennó* [1997] that, in order to produce a runaway greenhouse regime from an equilibrium solution, the finite amplitude perturbation must be large enough to produce a surface temperature larger than a critical value which corresponds to the unstable solution of *Nakajima et al.* [1992]. The initial perturbation utilized here for activating the runaway state for $1300 \leq S \leq 1570\mathrm{Wm}^{-2}$ in our GCM is quite huge; it is the runaway solution at $S = 1600\mathrm{Wm}^{-2}$. At the moment, we have not been able to determine a minimal magnitude of perturbation necessary to produce a runaway greenhouse state

from an equilibrium solution. In other words, it is required to figure out the GCM equivalent for the unstable equilibrium solution of *Nakajima et al.* [1992].

The critical values of solar constant at which the number of equilibrium state changes as shown in Figure 3a may vary according to the model configurations, such as the value of albedo, the details of the radiation scheme, and especially, the radiation effect of cloud which is excluded in the present study. However, the importance of our results is that we have exemplified the possibility of the coexistence of the ice-covered state, the partially ice-covered state, and the runaway greenhouse state, for a given, common solar constant value. The actual state to be realized at a particular value of solar constant depends on the initial condition and how the solar constant is varied. Our result shows that the runaway greenhouse state, which cannot be represented by previous EBMs [e.g., *Budyko*, 1969], is located not very far from the partially ice-covered or the globally ice-covered state in the climate regime diagram. Although the results of those previous EBMs are usually referred to as the standard climate regime diagram, it should be noted that their diagrams are missing an important regime: the runaway greenhouse state.

Acknowledgments

The authors wish to express their thanks to G. R. North and an anonymous reviewer for valuable comments on the original manuscript. The numerical codes and software environments were constructed using the resources of GFD DENNOU Club (URL; http://www.gfd-dennou.org). The calculations were performed by SX-6 at the National Institute of Environmental Science. One of the authors (MI) was supported by Grant-in-Aid for Young Scientists (B) of the Japan Society for the Promotion of Science.

References

Abe, Y., A. Numaguti, G. Komatsu, and Y. Kobayashi (2005), Four climate regimes on a land planet with wet surface: Effects of obiquity change and implications for ancient Mars, *Icarus*, *178*, 27–39.

Baum, S. K., and T. J. Crowley (2001), GCM respnonse to late Precambrian ($\sim$ 590Ma) ice-covered continents, *Geophys. Res. Lett.*, *28*, 583–586.

Budyko, M. I. (1969), The effect of solar radiation variations on the climate of the Earth, *Tellus*, *21*, 611-619.

Cahalan, R. F., and G. R. North (1979), A stability theorem for energy-balance climate models, *J. Atmos. Sci.*, *36*, 1178-1188.

Delworth, T. L., and S. Manabe (1988), The influence of potential evaporation on the variabilities of simulated soil wetness and climate, *J. Clim.*, *1*, 523-547.

Held, I. M., and M. J. Suarez (1974), Simple albedo feedback models of the icecaps, *Tellus*, *26*, 613-629.

Hoffman, P. F., A. J. Kaufman, G. P. Halverson, and D. P. Schrag (1998), A neoproterozoic snowball Earth, *Science*, *281*, 1342-1346.

Ingersoll, A. P. (1969), The runaway greenhouse: A history of water on Venus, *J. Atmos. Sci.*, *26*, 1191-1198.

Ishiwatari, M., K. Nakajima, S. Takehiro, and Y.-Y. Hayashi (1998), The dependency of the strucure of the three-dimensional gray atmosphere on the solar constant and the runaway greenhouse states, *Nagare Multimedia*, http://www.nagare.or.jp/mm/98/ishiwata/index.htm.

Ishiwatari, M., S. Takehiro, K. Nakajima, and Y.-Y. Hayashi (2002), A numerical study on appearance of the runaway greenhouse state of a three-dimensional gray atmosphere, *J. Atoms. Sci.*, *59*, 3223-3238.

Komabayashi, M. (1967), Discrete equilibrium temperatures of a hypothetical planet with the atmosphere and the hydrosphere of one component-two phase system under constant solar radiation, *J. Meteorol. Soc. Jpn.*, *45*, 137-139.

Lee, W.-H., and G. R. North (1995), Small icecap instability in the presence of fluctuations. *Clim. Dyn.*, *11*, 242-246.

Li, Z.-X., K. Ide, H. Le Treut, and M. Ghil (1997), Atmospheric radiative equilibria in a simple column model, *Clim. Dyn.*, *13*, 429-440.

Lindzen, R.S., and B. Farrell (1977), Some realistic modifications of simple climate models, *J. Atmos. Sci.*, *34*, 1487-1501.

Manabe, S., J. Smagorinsky, and R. F. Strickler (1965), Simulated climatology of a general circulation model with a hydrologic cycle, *Mon. Weather Rev.*, *93*, 769-798.

Nakajima, S., Y.-Y. Hayashi, and Y. Abe (1992), A study on the "Runaway Greenhouse Effect" with a one-dimensional radaiative-convective equilibrium model, *J. Atmos. Sci.*, *49*, 2256-2266.

North, G. R. (1975), Analytical solution to a simple climate model with diffusive heat transport, *J. Atmos. Sci.*, *32*, 1301–1307.

North, G. R. (1984), The small ice cap instability in diffusive climate models, *J. Atmos. Sci.*, *41*, 3390–3395.

Rennó, N.O. (1997), Multiple equilibria in radiative-convective atmospheres, *Tellus, Ser. A*, *49*, 423-438.

Satoh, M. (1994), Hadley circulations in radiative-convective equilibrium in an axially symmetric atmosphere, *J. Atmos. Sci.*, *51*, 1947-1968.

Sellers, W. D. (1969), A climate model based on the energy balance of the Earth-atmosphere system, *J. Appl. Meteorol.*, *8*, 392-400.

Sugiyama, M., P. H. Stone, and K. A. Emanuel (2005), The role of relative humidity in radiative convective equilibrium, *J. Atmos. Sci.*, *62*, 2001-2011.

List of Figures

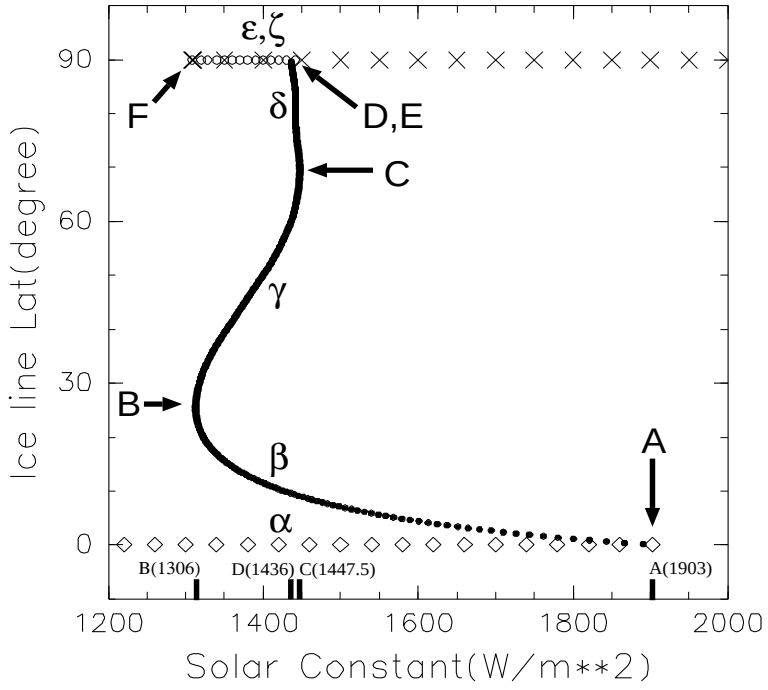

Figure 1: Relationship between solar constant and ice line latitude obtained by the EBM: open circle, ice-free equilibrium solution; solid circle, a partially ice-covered equilibrium solution; diamond, a globally ice-covered equilibrium solution; and cross, a runaway greenhouse solution. Points A to F represent critical points, and line segments α to ζ represent branches of equilibrium solutions. Numbers in parentheses on the abscissa indicate calculated values of solar constant for critical points A to D.

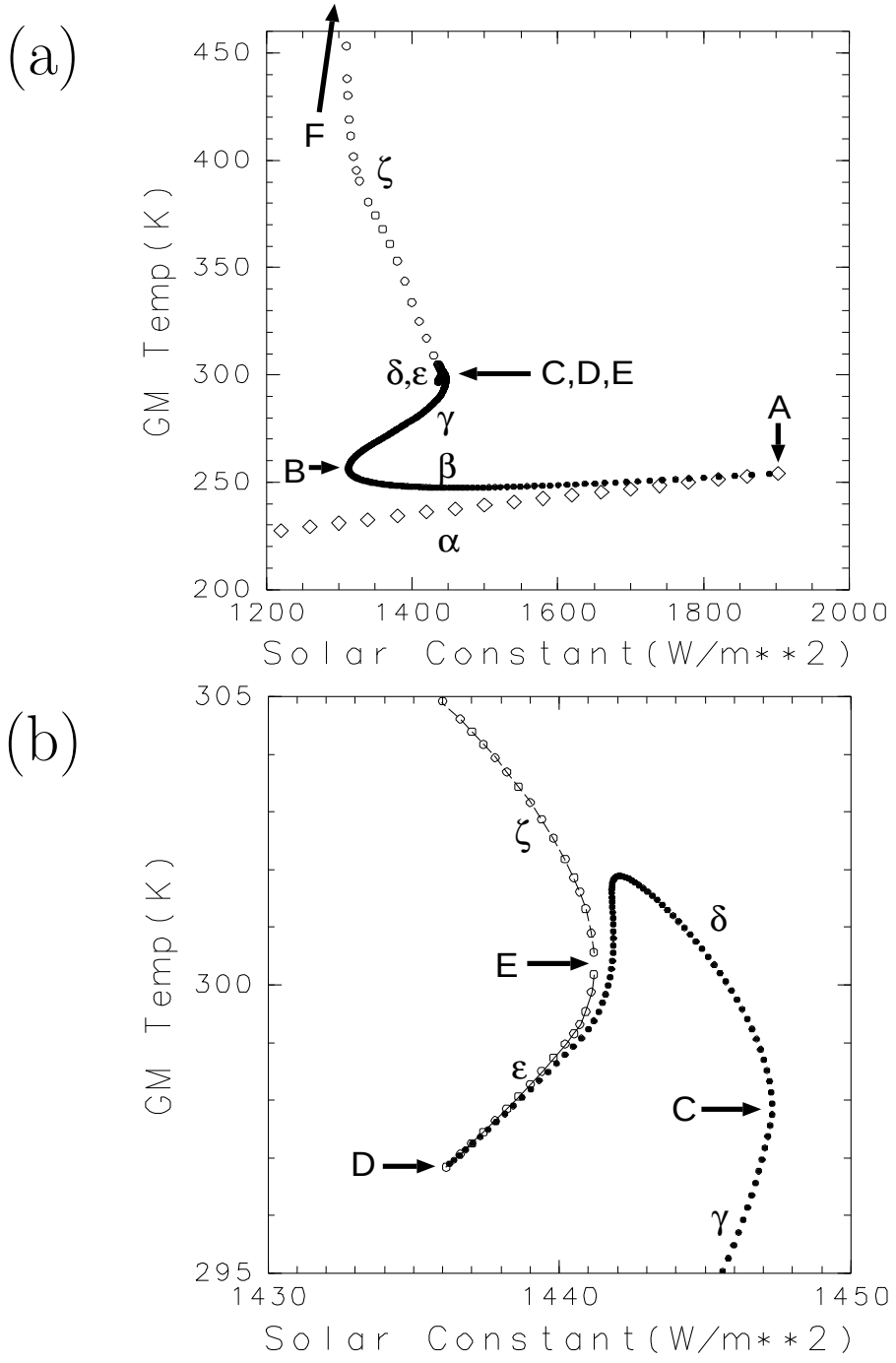

Figure 2: (a) Relationship between solar constant and global mean surface temperature obtained by the EBM. Symbols are the same as in Figure 1, except that the case for the runaway greenhouse state is not plotted. (b) An enlarged view of Figure 2a near critical points C, D, and E.

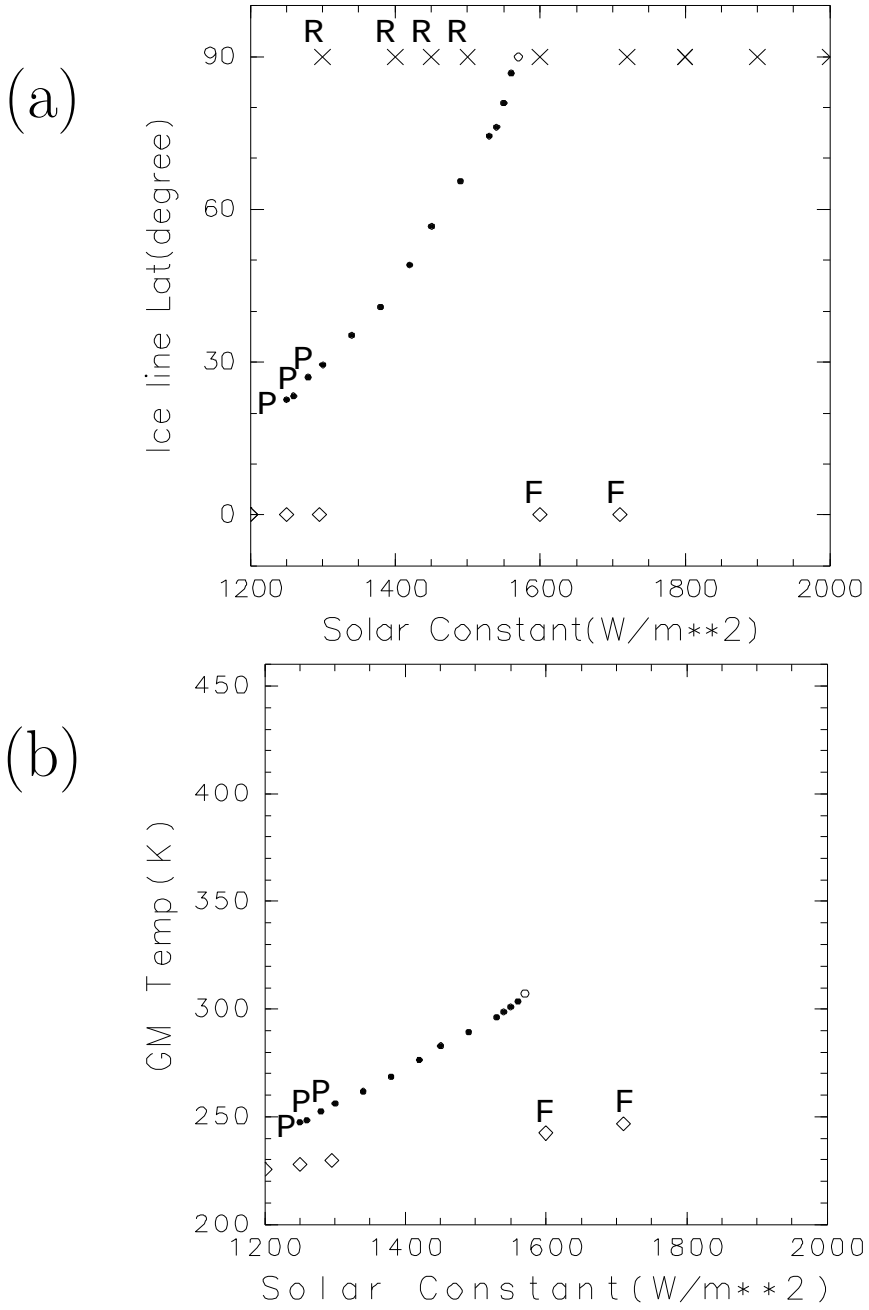

Figure 3: (a) Relationship between solar constant and ice line latitude obtained by the GCM. (b) Relationship between solar constant and global mean surface temperature obtained by the GCM. The symbols are the same as those in Figure 1. F represents the results for runs in which the initial condition is the ice-covered solution calculated with $S = 1000$ Wm^{-2}, R represents the results for those in which the initial condition is the runaway greenhouse solution obtained with $S = 1600$ Wm^{-2}, and P represents the results obtained by decreasing S gradually starting from a partially ice-covered solution obtained using $S = 1300$ Wm^{-2}. Points with no labels represent the results whose initial condition is the isothermal state (280K).

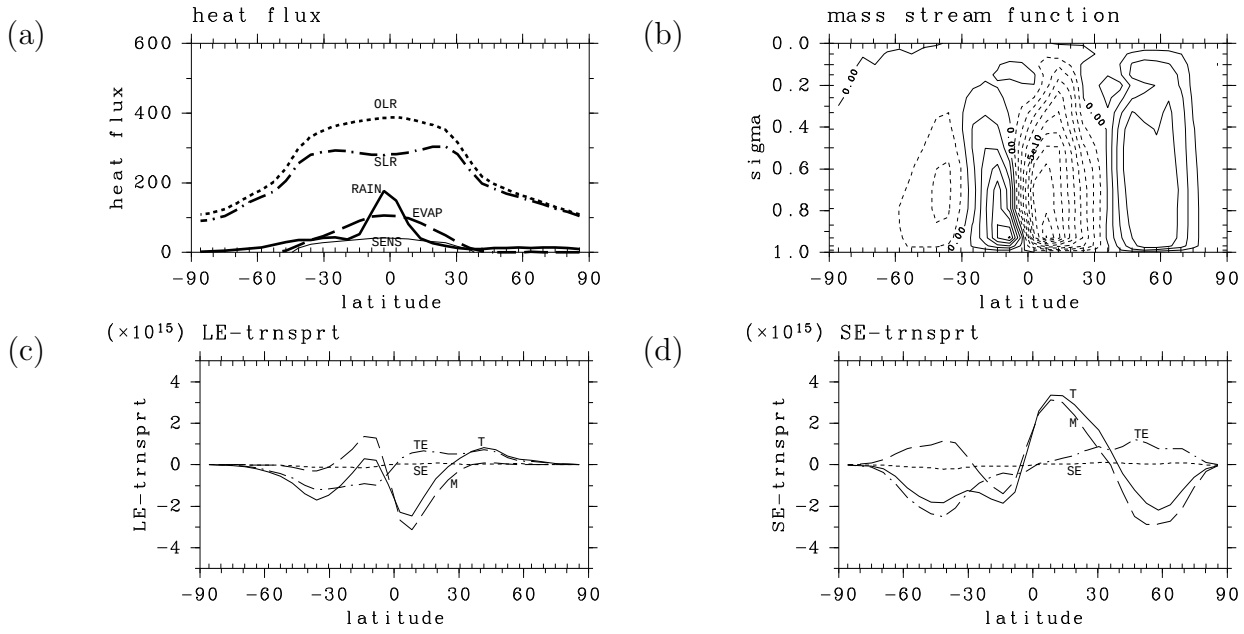

Figure 4: Temporal and zonal mean meridional structure of the circulation fields obtained by the GCM for $S = 1380$ Wm^{-2}. (a) The meridional distributions of vertical energy fluxes. Thick solid line (also labeled as RAIN) is condensation heating rate, dashed line (EVAP) is evaporation heat flux, dotted line (OLR) is outgoing longwave radiation, dashed-dotted line (SLR) is net long wave radiation at the surface, and thin solid line (SENS) is sensible heat flux. Unit is Wm^{-2}. (b) Mass stream function. Contour interval is 1.0×10^{10} kg s^{-1}. (c) Latitudinal latent heat transport, and (d) sensible heat transport. Unit is W. Thick line (T) is total transport, dashed line (M) is zonal and time mean meridional transport, dotted line (SE) is steady eddy transport, and dashed-dotted line (TE) is time-dependent eddy transport. Refer to *Ishiwatari et al.* [2002] for details on the definition of heat transport.

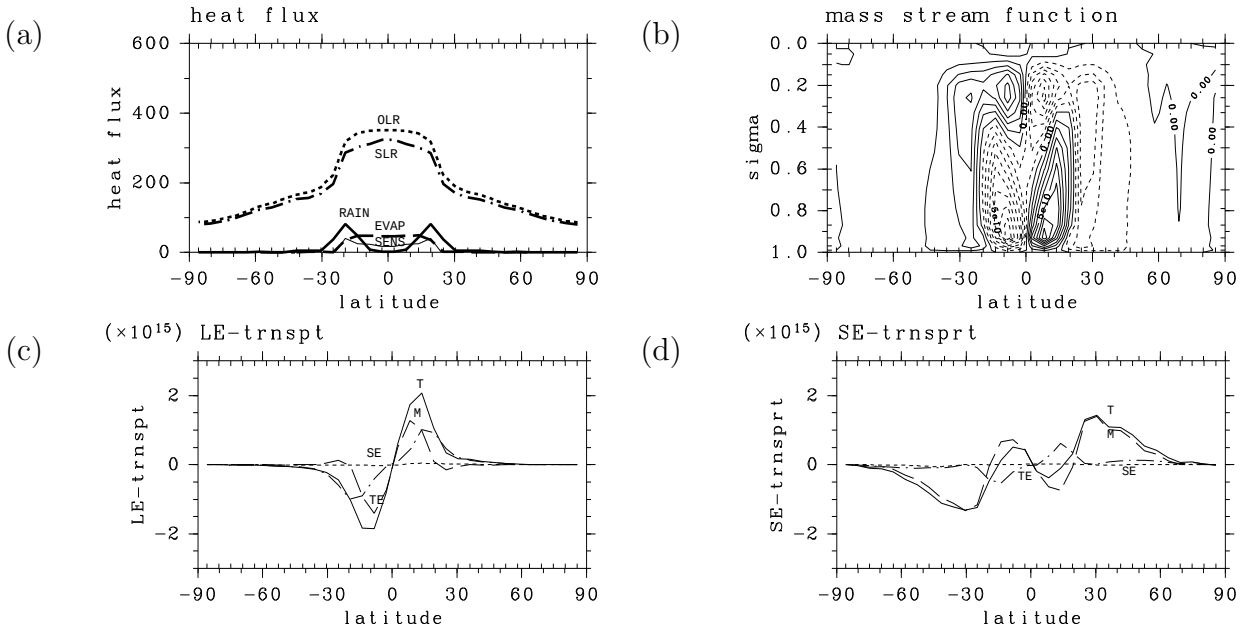

Figure 5: Same as Figure 4, but for the case of $S = 1250$ Wm^{-2}.

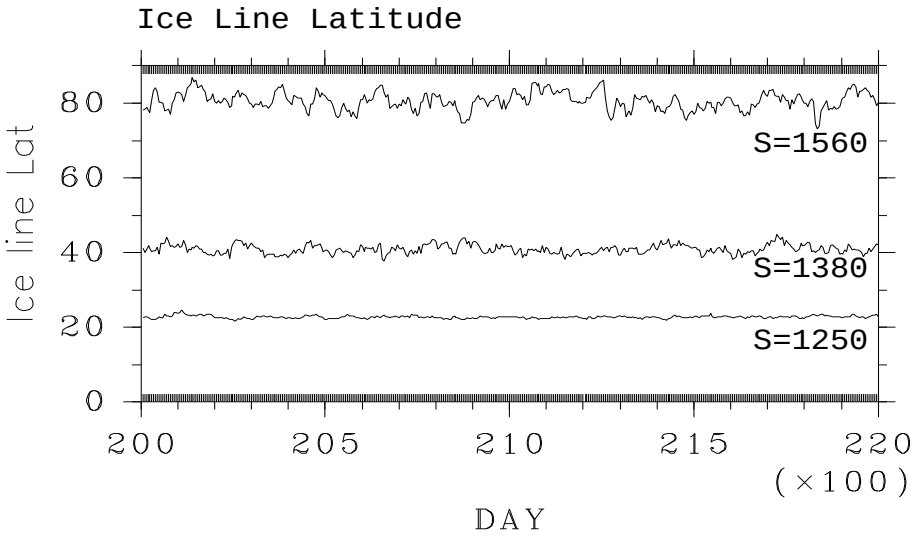

Figure 6: Time series of the ice line latitudes obtained by the GCM. The averaged latitudes of the northern and southern lines are shown. The upper, middle, and lower lines correspond to $S = 1560, 1380$, and 1250 Wm^{-2}, respectively.